Complete measurement and multiplexing of orbital angular momentum Bell states

Ling-Jun Kong,[1,3,5] Yongnan Li,[2,*] Rui Liu,[2] Wen-Rong Qi,[2] Qiang Wang,[2] Zhou-Xiang Wang,[2] Shuang-Yin Huang,[2] Yu Si,[2] Chenghou Tu,[2] Wei Hu,[1,4,5] Fei Xu,[1,4,5] Yan-Qing Lu,[1,4,5] and Hui-Tian Wang[1,3,5,†]

[1]*National Laboratory of Solid State Microstructures, Nanjing University, Nanjing 210093, China*

[2]*Key Laboratory of Weak-Light Nonlinear Photonics and School of Physics, Nankai University, Tianjin 300071, China*

[3]*School of Physics, Nanjing University, Nanjing 210093, China*

[4]*College of Engineering and Applied Sciences, Nanjing University, Nanjing 210093, China*

[5]*Collaborative Innovation Center of Advanced Microstructures, Nanjing University, Nanjing 210093, China*

(Received 1 November 2018; published 14 August 2019)

Orbital angular momentum (OAM) entanglement states have great potential in enhancing the information capacity in quantum communications. To make full use of the OAM degree of freedom, the measurement and distinction of OAM Bell states become a key step that needs to be accomplished. However, there is still no solution to achieve complete distinction of OAM Bell states at the single-photon level. Here we demonstrate the complete OAM Bell-state measurement without auxiliary photons by using linear optics. Furthermore, we propose a quantum communication network via OAM Bell-state multiplexing, perform a proof-of-principle experiment in the first- and second-order OAM subspaces for two users, and achieve average success probabilities of obtaining information of 91.6% for User-I and 89.1% for User-II. In principle, our scheme allows more users to be added by using high-order OAM Bell states. Our research extends the manipulation method for high-dimensional quantum states and paves the way for the application of OAM multiplexing in quantum communications.

DOI: 10.1103/PhysRevA.100.023822

I. INTRODUCTION

Multiplexing is natural and essential to increase the capacity of carrying information, and for scalability in not only classical but also quantum communications. One of the keys to achieve the multiplexing is the need for high-dimensional resources. In the field of quantum communication, the heralded single-photon multiplexing has been explored by using various degrees of freedom of photons, such as path [1,2], temporal [3,4], and spectral [5]. Orbital angular momentum (OAM) [6], as a novel degree of freedom of photon, should be an extremely important resource of quantum information, because it can form a Hilbert space with dimension of no upper limit in principle. Since the OAM entanglement was first demonstrated [7], it has attracted much attention in quantum optics [8–17]. It has been regarded as the most promising candidate to provide access to the high-dimensional quantum states [18,19]. So the OAM multiplexing is an effective way to increase the capacity of information in quantum communication.

To further enhance the ability of information carried by single-photon OAM states, one should create the OAM Bell states for encoding; in particular, it is absolutely necessary to achieve its complete measurement for decoding. However, only one of the four OAM Bell states in every individual subspace can be distinguished from others with Hong-Ou-Mandel (HOM) interference effect [20], because other three of the four OAM Bell states possess the degenerate measurement result. To make full use of OAM Bell state multiplexing, it is a bottleneck to solve the problem of the complete OAM Bell-state measurement at the single-photon level.

Here we propose a scheme for the first realization of the complete OAM Bell-state measurement in every individual subspace without auxiliary photons by using linear optics. The key of our idea is to break the degeneracy of coincidence measurements of four OAM Bell-states with ancillary spin dimension. Based on the complete OAM Bell-state measurement, we conceive a quantum network model of the OAM Bell-state multiplexing. We confirm our idea with a proof-of-principle experiment in the first- and second-order OAM subspaces for two users.

II. PREPARATION AND MEASUREMENT OF ORBITAL ANGULAR MOMENTUM BELL STATES

As shown in Fig. 1(a), the hyperentangled photon source is generated by pumping two 0.6-mm-thick BBO nonlinear crystals with optic axes aligned in perpendicular planes. Under the type-I phase matching, down-converted photons at a degenerate wavelength of 810 nm in a 1.5° half-opening angle cone are produced. Thus the spin-OAM hyperentangled state can be generated via the spontaneous parametric down-conversion (SPDC) process and a half wave plate (HWP) as [7,21,22]

$$\left|\Theta_1^m\right\rangle = |\Psi_{\text{spin}}^+\rangle \otimes |\Psi_m^+\rangle. \tag{1}$$

Here $|\Psi_{\text{spin}}^+\rangle = (|H\rangle_A|V\rangle_B + |V\rangle_A|H\rangle_B)/\sqrt{2}$ is one of four spin Bell states. H (V) represents horizontal (vertical)

*liyongnan@nankai.edu.cn
†htwang@nju.edu.cn

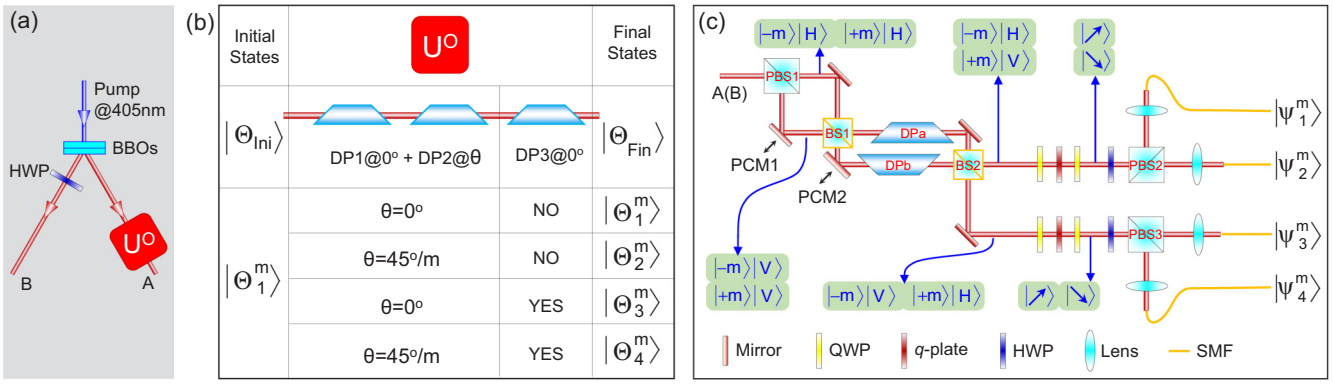

FIG. 1. Experimental schematic for complete measurement of OAM Bell states. (a) Hyperentangled source and the unitary operator U^o for manipulating the OAM states. The pump light is a fundamental-mode Gaussian femtosecond (fs) pulsed laser with a power of ∼500 mW, a central wavelength of 405 nm, a pulse duration of ∼140 fs, a repetition rate of ∼80 MHz, and a beam waist of $\omega_0 \sim 1.5$ mm. The beam waist is located in the central plane of the nonlinear crystals. A paired 0.6-mm-thick type-I phase-matched β-BaBO^3 (BBO) crystals with optic axes aligned in perpendicular planes is used to generate the entangled photon-pair at a wavelength of 810 nm. A HWP in the path B is used to convert the polarization state as $|H\rangle \leftrightarrow |V\rangle$. (b) Detail of the $U(2)$ unitary operator U^o and its function. U^o is composed of three Dove prisms (DPs). θ is the relative orientation angle between DP1 and DP2. To realize the conversion of the mth-order OAM Bell state, θ should be set at $\theta = 45^\circ/m$. (c) OAM Bell-state analyzer. Photon A (or B) of an OAM Bell state $\{|\Theta_i^m\rangle\}$ $(i = 1, \ldots, 4)$ meets PSB1 first. Photon in the state $|-m\rangle|H\rangle$ or $|+m\rangle|H\rangle$ ($|-m\rangle|V\rangle$ or $|+m\rangle|V\rangle$) will pass through (be reflected by) PBS1. Then the reflected and transmitted photon enter a modified MZ interferometer, which is composed of two beam splitters (BSs) and two DPs, from different entrances. The relative orientation angle between DPa and DPb is set to be $45^\circ/m$. After the modified MZ interferometer, photons in both states $|-m\rangle|H\rangle$ and $|+m\rangle|V\rangle$ ($|-m\rangle|V\rangle$ and $|+m\rangle|H\rangle$) exit from the right (bottom) output port of BS2. A q plate sandwiched by two quarter-wave plates (QWPs), a HWP@22.5°, and a PBS are used together to project the state $\{|\psi_k^m\rangle\}$ $(k = 1, \ldots, 4)$ into the fundamental Gauss mode, which is collected by the SMF.

polarization, and subscript A (B) labels the photon path (photon in the path A or B is abbreviated as photon A or B below). In the individual mth-order OAM subspace, four OAM Bell states are written as

$$|\Psi_m^{\pm}\rangle = (|+m\rangle_A|-m\rangle_B \pm |-m\rangle_A|+m\rangle_B)/\sqrt{2},$$
$$|\Phi_m^{\pm}\rangle = (|+m\rangle_A|+m\rangle_B \pm |-m\rangle_A|-m\rangle_B)/\sqrt{2}, \quad (2)$$

where $|\pm m\rangle$ represent photon states with OAMs of $\pm m\hbar$. $|\Theta_1^m\rangle$ can be converted into any one of other three spin-OAM hyperentangled states, $|\Theta_2^m\rangle$ $(=|\Psi_{\rm spin}^+\rangle \otimes |\Psi_m^-\rangle)$, $|\Theta_3^m\rangle$ $(=|\Psi_{\rm spin}^+\rangle \otimes |\Phi_m^+\rangle)$, or $|\Theta_4^m\rangle$ $(=|\Psi_{\rm spin}^+\rangle \otimes |\Phi_m^-\rangle)$ by performing the suitable unitary operation on OAM state of photon A, as shown in Fig. 1(b), as follows:

(i) $|\Theta_1^m\rangle \Rightarrow |\Theta_2^m\rangle$ requires two $U(2)$ unitary operations of $|\pm m\rangle_A \rightarrow \pm j|\pm m\rangle_A$, which can be realized with a pair of Dove prisms (DPs) oriented at an angle $45^\circ/m$ with respect to each other [20,23].

(ii) $|\Theta_1^m\rangle \Rightarrow |\Theta_3^m\rangle$ requires one $U(2)$ unitary operation of $|+m\rangle_A \leftrightarrow |-m\rangle_A$, which can be realized with a DP.

(iii) $|\Theta_1^m\rangle \Rightarrow |\Theta_4^m\rangle$ requires three $U(2)$ unitary operations of $|\pm m\rangle_A \rightarrow \pm j|\pm m\rangle_A$ and $|+m\rangle_A \leftrightarrow |-m\rangle_A$, simultaneously.

Any hyperentangled state $|\Theta_i^m\rangle$ $(i = 1, 2, 3, 4)$ is in fact a superposition of the basis set $\{|\phi_k^m\rangle_A|\phi_{k'}^m\rangle_B\}$ $(k, k' = 1, \ldots, 4)$, where $|\phi_1^m\rangle = |-m\rangle|H\rangle$, $|\phi_2^m\rangle = |+m\rangle|V\rangle$, $|\phi_3^m\rangle = |-m\rangle|V\rangle$, and $|\phi_4^m\rangle = |+m\rangle|H\rangle$ (see Appendix for details). When we project the hyperentangled states into the basis set $\{|\phi_k^m\rangle_A|\phi_{k'}^m\rangle_B\}$ and carry out the coincidence measurements, $|\Theta_1^m\rangle$ and $|\Theta_2^m\rangle$ ($|\Theta_3^m\rangle$ and $|\Theta_4^m\rangle$) give the degenerate coincidence count results (see Fig. 5 in Appendix), implying that we cannot distinguish the OAM Bell states completely. Clearly, seeking a suitable basis set is a key issue to break the degeneracy of coincidence measurement for different OAM Bell states. We indeed find a series of $U(4)$ unitary operations with linear optics only (see Appendix). For the feasibility in experiment, we select the following $U(4)$ operation to transform the projective basis set $\{|\phi_k^m\rangle\}$ into $\{|\psi_k^m\rangle\}$ as

$$\begin{pmatrix} |\psi_1^m\rangle \\ |\psi_2^m\rangle \\ |\psi_3^m\rangle \\ |\psi_4^m\rangle \end{pmatrix} = U(4) \begin{pmatrix} |\phi_1^m\rangle \\ |\phi_2^m\rangle \\ |\phi_3^m\rangle \\ |\phi_4^m\rangle \end{pmatrix} = \frac{1}{\sqrt{2}} \begin{pmatrix} |\phi_1^m\rangle + |\phi_2^m\rangle \\ |\phi_1^m\rangle - |\phi_2^m\rangle \\ |\phi_3^m\rangle + |\phi_4^m\rangle \\ |\phi_3^m\rangle - |\phi_4^m\rangle \end{pmatrix}. \quad (3)$$

Thus, we can rewrite four hyperentangled states $|\Theta_i^m\rangle$ under the projective basis set $\{|\psi_k^m\rangle_A|\psi_{k'}^m\rangle_B\}$ as

$$|\Theta_1^m\rangle \propto +|\psi_1^m\rangle_A|\psi_1^m\rangle_B - |\psi_2^m\rangle_A|\psi_2^m\rangle_B + |\psi_3^m\rangle_A|\psi_3^m\rangle_B - |\psi_4^m\rangle_A|\psi_4^m\rangle_B, \quad (4a)$$
$$|\Theta_2^m\rangle \propto +|\psi_2^m\rangle_A|\psi_1^m\rangle_B - |\psi_1^m\rangle_A|\psi_2^m\rangle_B + |\psi_4^m\rangle_A|\psi_3^m\rangle_B - |\psi_3^m\rangle_A|\psi_4^m\rangle_B, \quad (4b)$$
$$|\Theta_3^m\rangle \propto +|\psi_3^m\rangle_A|\psi_1^m\rangle_B + |\psi_4^m\rangle_A|\psi_2^m\rangle_B + |\psi_1^m\rangle_A|\psi_3^m\rangle_B + |\psi_2^m\rangle_A|\psi_4^m\rangle_B, \quad (4c)$$
$$|\Theta_4^m\rangle \propto +|\psi_4^m\rangle_A|\psi_1^m\rangle_B + |\psi_3^m\rangle_A|\psi_2^m\rangle_B + |\psi_2^m\rangle_A|\psi_3^m\rangle_B + |\psi_1^m\rangle_A|\psi_4^m\rangle_B. \quad (4d)$$

Clearly, Eqs. (4) show that any hyperentangled state is a unique superposition of four among 16 possible combinations under the basis set $\{|\psi_k^m\rangle_A|\psi_{k'}^m\rangle_B\}$. That is to say, when carrying out the local Bell-state measurement, all the OAM Bell

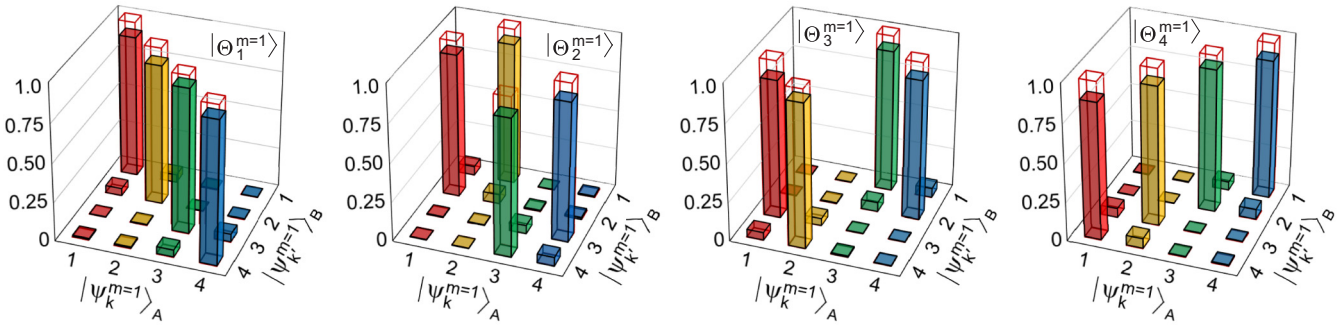

FIG. 2. Experimental results of four first-order OAM Bell-state measurements. The coincidence measurement is done under the projective basis set of $\{|\psi_k^{m=1}\rangle_A|\psi_{k'}^{m=1}\rangle_B\}$ $(k, k' = 1, ..., 4)$. The empty bars are theoretical values. The vertical axis represents the normalized coincidence counts.

states in the mth-order OAM subspace can be distinguished completely.

Based on the above theoretical analysis, we design an OAM Bell-state analyzer for distinguishing completely all the OAM Bell states, as shown in Fig. 1(c) (see Appendix for details on evolution of the photon states). In our OAM Bell-state analyzer, photon A (or B) of the photon pair will meet a polarizing beam splitter (PBS1). We use a piezo-controlled mirror (PCM1) to control the equal optical paths of the two arms between PBS1 and BS1 (the first beam splitter). BS1 and BS2 form a modified Mach-Zehnder (MZ) interferometer, which contains a pair of DPs (DPa and DPb) oriented at an angle of $45^\circ/m$ with each other.

We can actively control the optical path difference between two arms of the MZ interferometer by PCM2 to ensure that photons in the states $|\phi_1^m\rangle$ and $|\phi_3^m\rangle$ ($|\phi_2^m\rangle$ and $|\phi_4^m\rangle$) emit from different output ports of BS2. In fact, BS1 and BS2 form a two-input and two-output OAM beam splitter [23] (OAM-BS and see Appendix for its detail), which allows the photons in the $|+m\rangle$ ($|-m\rangle$) state to be transmitted (reflected). The stability of the interferometer is controlled by a servo system (Appendix). An $m/2$-order q plate [24–26] sandwiched between two quarter-wave plates (QWPs) transforms the states $|\psi_1^m\rangle$ and $|\phi_2^m\rangle$ (or $|\phi_3^m\rangle$ and $|\phi_4^m\rangle$) into the fundamental Gaussian mode with polarizations of $|\nearrow\rangle$ and $|\searrow\rangle$, as shown in Fig. 1(c). $|\nearrow\rangle \propto |H\rangle + |V\rangle$ and $|\searrow\rangle \propto |H\rangle - |V\rangle$ can be separated with a combination of a PBS and a HWP@22.5° (HWP: half wave plate). As shown in Fig. 1(c), photons in the four basis states $|\psi_k^m\rangle$ exit from four output ports of PBS2 and PBS3, respectively. A single-mode fiber (SMF) collects the photons in the state of fundamental Gaussian mode and filters others. We experimentally measure 16 possible coincidence counts between the photon A and B for $m = 1$ (Fig. 2). The result shows that only the four unique combinations give the coincidence count signals for either one of the input spin-OAM hyperentangled Bell states $|\Theta_i^{m=1}\rangle$. Clearly, we achieve the completely deterministic OAM Bell-state measurement. We also use the signal-to-noise ratio (SNR) of a state as the ratio between the sum of coincidence counts for the four actual states and that for the other twelve states to characterize the quality of states [21]. The measured SNRs of the four spin-OAM hyperentangled Bell states are $\mathrm{SNR}_{|\Theta_1^{m=1}\rangle} = 9.61$, $\mathrm{SNR}_{|\Theta_2^{m=1}\rangle} = 8.98$, $\mathrm{SNR}_{|\Theta_3^{m=1}\rangle} = 9.02$, and $\mathrm{SNR}_{|\Theta_4^{m=1}\rangle} = 8.07$.

III. QUANTUM COMMUNICATION NETWORK WITH ORBITAL ANGULAR MOMENTUM BELL-STATE MULTIPLEXING

As mentioned above, the OAM-BS can separate the OAM states in an mth-order individual subspace by setting a pair of DPs oriented at an angle of $45^\circ/m$ with each other. One should note that OAM-BS can also separate the OAM states into two different-order (m'th- and m''th-order) individual subspaces by setting a pair of DPs oriented at an angle of $\pi/(2|m' - m''|)$ with each other [23]. This means that the OAM-BS can be used to demultiplex the OAM Bell states in different subspaces. Consequently, we present a conceptual schematic of the quantum network based on OAM Bell-state multiplexing, as shown in Fig. 3(a). A high-dimensional OAM entanglement source is located in Building 1. One of two-photon pairs is used to perform the projective measurement; the detected signal (as a trigger) are delivered to every user through the trigger channel. Another photon is used as a carrier of information. The different-order OAM Bell states carrying independent data streams are demultiplexed by the OAM-BSs and then distributed to different users in Building 2. The number of users is unlimited in principle because the OAM degree of freedom can form an infinite-dimensional Hilbert space. Users decode their messages by performing the projective measurement in the quantum channel by the trigger.

We present an experimental scheme and carry out the proof-of-principle test in this quantum network with the OAM Bell-state multiplexing, in which the first- and second-order OAM states are utilized, as shown in Fig. 3(b). The entangled photon pairs are generated from the SPDC process (also see Methods for its details). Photon B in the two-photon pair meets an OAM-BS to separate the first- and second-order OAM states from each other. After implementing the projective measurements on photon B with our OAM Bell-state analyzer shown in Fig. 1(c), the detected signal (as a trigger) is sent to every user through the trigger channel. Alice (sender) encodes two-bit messages by operating photon A with the operator U^o, and an OAM BS is also used to separate the first- and second-order OAM states from each other. User-I (User-II) performs the first-order (second-order) OAM Bell-state measurement by using our OAM Bell-state analyzer with the trigger and finally decodes the two-bit messages, as shown in Fig. 3(b).

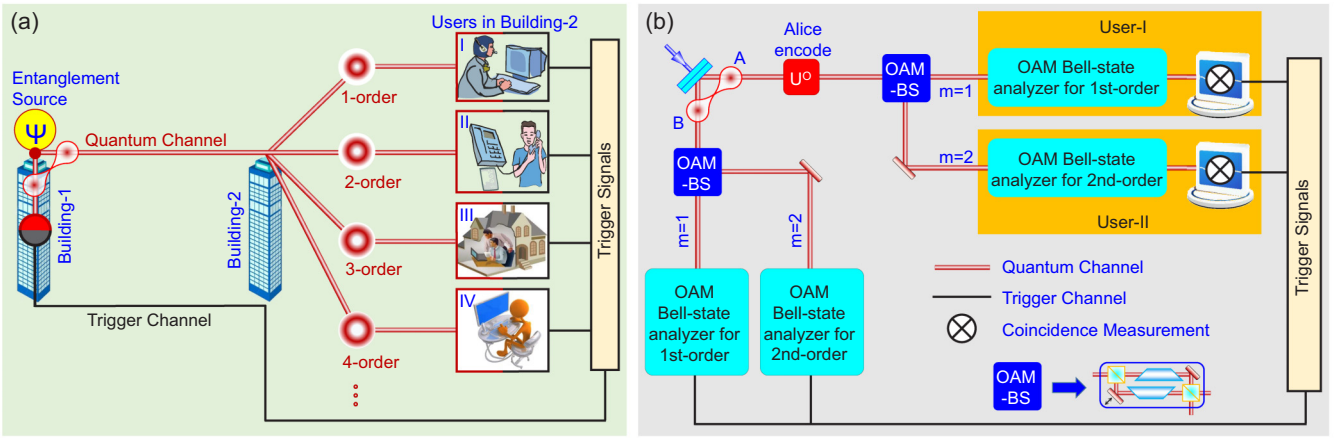

FIG. 3. Schematic of quantum communication network. (a) Conceptual diagram of quantum communication network with OAM Bell-state multiplexing. (b) Experimental setup of the quantum communication network with OAM Bell-state multiplexing.

The measured data (Fig. 4) reveal that the message transfers from Alice to different users are independent. There are two ways of message transmission from Alice to different users. First, every time Alice sends only one of the four first-order OAM Bell states to only User-I, or only one of the four second-order OAM Bell states to only User-II. The tested result for eight different cases in Fig. 4(a) shows the average success probabilities of 91.6% for User-I and of 89.1% for User-II. Second, Alice sends one of the four first-order Bell states to User-I and one of the four second-order Bell states to User-II simultaneously; the result shows that the success probabilities are 92.8% (90.3%) for User-I (User-II) and verifies that there is almost no crosstalk between the users in Fig. 4(b). The noise mainly comes from the imperfections of optical elements, alignment, and input states. We should emphasize that our proof-of-principle test were implemented on a 1.2×2.4 m^2 optical table covered with a black box, so the turbulence effect could be ignored. However, to make our quantum network more practical for covering long distances, the turbulence effect in free space and/or propagation characteristics in optical fiber should be studied further. Related research can be found in Refs. [27–31].

In our experiment, the success probability for $m = 1$ is 91.6%, while the success probability for $m = 2$ is 89.1%, which is a little less than that for $m = 1$. One reason is that the experimental complexity scale for $m = 2$ becomes a little bigger than for $m = 1$. Another reason is that the brightness of the source of the photon pair for $m = 2$ is weaker than for $m = 1$, which makes alignment more difficult. To obtain better experimental results, we reduce noise as much as possible. All unnecessary light is turned off during the experiment. On the other hand, we make our photon-pair source as strong as possible. Although our experimental results are not perfect, they suffice to demonstrate our theory.

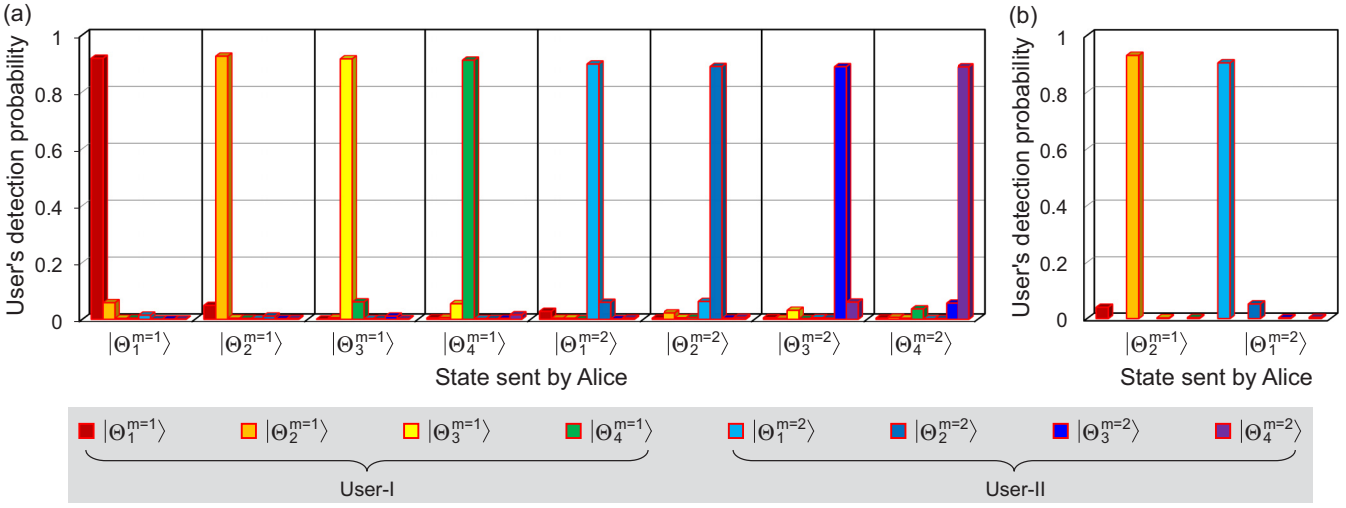

FIG. 4. Experimental results of quantum communication network with OAM Bell-state multiplexing. The horizontal axis represents states sent by Alice and the vertical axis represents the detection probabilities of users for different OAM Bell states. (a) Every time Alice sends only one of four OAM Bell states ($|\Theta_1^{m=1}\rangle$, $|\Theta_2^{m=1}\rangle$, $|\Theta_3^{m=1}\rangle$, $|\Theta_4^{m=1}\rangle$) to only User-I, or only one of four OAM Bell states ($|\Theta_1^{m=2}\rangle$, $|\Theta_2^{m=2}\rangle$, $|\Theta_3^{m=2}\rangle$, $|\Theta_4^{m=2}\rangle$) to only User-II. Average success probabilities are 91.6% for User-I and 89.1% for User-II. (b) Alice sends $|\Theta_2^{m=1}\rangle$ to User-I and $|\Theta_1^{m=2}\rangle$ to User-II, simultaneously.

IV. CONCLUSION

We have demonstrated a complete OAM Bell-state measurement by seeking the suitable unitary matrix performable by using only linear optics and breaking the degeneracy of four OAM Bell states in an ancillary polarization dimension. We then build a quantum information network with the OAM Bell-state multiplexing by using our OAM Bell-state analyzer. Different-order OAM Bell states carry independent messages sent to different users. We have carried out experiments with first- and second-order OAM states for a proof-of-principle test. This process is in fact multiplexing of superdense coding with a two-bit channel capacity based on the OAM Bell states [21,32,33]. Our experiments achieve the average success probabilities of ∼90% for User-I and User-II. To improve the performance of the entanglement source, more users can be added conveniently by cascading more OAM BSs and our OAM Bell-state analyzers because OAM has infinite dimensions in principle. Additionally, the idea of OAM Bell states multiplexing can also be applied to improve the ability of information process in quantum protocols, such as quantum teleportation [14,34–36] and quantum swapping [37–39]. Our research make photonic OAM more valuable in practical applications.

ACKNOWLEDGMENTS

This work was funded by the National Key R&D Program (2017YFA0303800, 2017YFA0303700) and the National Natural Science Foundation of China (11534006, 11374166). We acknowledge the support by Collaborative Innovation Center of Extreme Optics.

APPENDIX

1. Search for suitable projection states

When the pump light is a fundamental Gaussian mode, the high-dimensional spin-OAM hyperentangled state generated via the spontaneous parametric down-conversion (SPDC) and a half-wave plate (HWP) can be written as

$$\left|\Theta_1^m\right\rangle = |\Psi_{\rm spin}^+\rangle \otimes |\Psi_m^+\rangle. \tag{A1}$$

Here $|\Psi_{\rm spin}^+\rangle = (|H\rangle_A|V\rangle_B + |V\rangle_A|H\rangle_B)/\sqrt{2}$ is one of four spin Bell states. $H(V)$ represents horizontal (vertical) polarization. Subscript A (B) labels the photon path. $|\Psi_m^+\rangle$ is one of four OAM Bell states described as follows:

$$|\Psi_m^\pm\rangle = (|+m\rangle_A|-m\rangle_B \pm |-m\rangle_A|+m\rangle_B)/\sqrt{2}, \tag{A2a}$$

$$|\Phi_m^\pm\rangle = (|+m\rangle_A|+m\rangle_B \pm |-m\rangle_A|-m\rangle_B)/\sqrt{2}, \tag{A2b}$$

where $|+m\rangle$ ($|-m\rangle$) stands for a state of photon with an OAM of $+m\hbar$ ($-m\hbar$). Assume that $|\phi_1^m\rangle = |-m\rangle|H\rangle$, $|\phi_2^m\rangle = |+m\rangle|V\rangle$, $|\phi_3^m\rangle = |-m\rangle|V\rangle$, and $|\phi_4^m\rangle = |+m\rangle|H\rangle$ are the initial basis set. Thus, the spin-OAM hyperentangled state in mth-order subspace can be rewritten as

$$\begin{aligned}\left|\Theta_1^m\right\rangle \propto &+\left|\phi_1^m\right\rangle_A\left|\phi_2^m\right\rangle_B + \left|\phi_3^m\right\rangle_A\left|\phi_4^m\right\rangle_B \\ &+\left|\phi_4^m\right\rangle_A\left|\phi_3^m\right\rangle_B + \left|\phi_2^m\right\rangle_A\left|\phi_1^m\right\rangle_B.\end{aligned} \tag{A3a}$$

Similarly, the other three spin-OAM hyperentangled states, $|\Theta_2^m\rangle = |\Psi_{\rm spin}^+\rangle \otimes |\Psi_m^-\rangle$, $|\Theta_3^m\rangle = |\Psi_{\rm spin}^+\rangle \otimes |\Phi_m^+\rangle$, and $|\Theta_4^m\rangle = |\Psi_{\rm spin}^+\rangle \otimes |\Phi_m^-\rangle$, can be also rewritten as

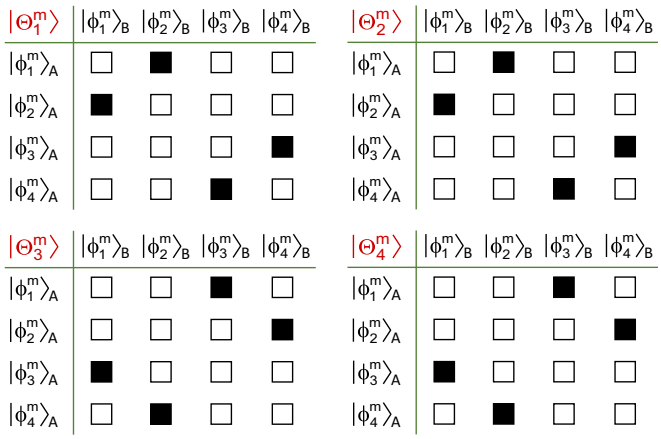

FIG. 5. The simulated results of coincidence measurements for $|\Theta_1^m\rangle$, $|\Theta_2^m\rangle$, $|\Theta_3^m\rangle$, and $|\Theta_4^m\rangle$ under the basis set $\{|\phi_k^m\rangle_A|\phi_{k'}^m\rangle_B\}$ $(k, k' = 1, ..., 4)$. The symbols □ (■) represent that the coincidence-measurement possibility is zero (nonzero).

$$\begin{aligned}\left|\Theta_2^m\right\rangle \propto &+\left|\phi_1^m\right\rangle_A\left|\phi_2^m\right\rangle_B + \left|\phi_3^m\right\rangle_A\left|\phi_4^m\right\rangle_B \\ &-\left|\phi_4^m\right\rangle_A\left|\phi_3^m\right\rangle_B - \left|\phi_2^m\right\rangle_A\left|\phi_1^m\right\rangle_B,\end{aligned} \tag{A3b}$$

$$\begin{aligned}\left|\Theta_3^m\right\rangle \propto &+\left|\phi_2^m\right\rangle_A\left|\phi_4^m\right\rangle_B + \left|\phi_4^m\right\rangle_A\left|\phi_2^m\right\rangle_B \\ &+\left|\phi_1^m\right\rangle_A\left|\phi_3^m\right\rangle_B + \left|\phi_3^m\right\rangle_A\left|\phi_1^m\right\rangle_B,\end{aligned} \tag{A3c}$$

$$\begin{aligned}\left|\Theta_4^m\right\rangle \propto &+\left|\phi_2^m\right\rangle_A\left|\phi_4^m\right\rangle_B + \left|\phi_4^m\right\rangle_A\left|\phi_2^m\right\rangle_B \\ &-\left|\phi_1^m\right\rangle_A\left|\phi_3^m\right\rangle_B - \left|\phi_3^m\right\rangle_A\left|\phi_1^m\right\rangle_B.\end{aligned} \tag{A3d}$$

When projecting the hyperentangled states into the basis set $\{|\phi_k^m\rangle_A|\phi_{k'}^m\rangle_B\}$ $(k, k' = 1, \ldots, 4)$ and performing the coincidence measurement between photons A and B, the results shown in Fig. 5 will be obtained in principle. As shown in Fig. 5, we can find that $|\Theta_1^m\rangle$ and $|\Theta_2^m\rangle$ (or $|\Theta_3^m\rangle$ and $|\Theta_4^m\rangle$) have the same coincidence counts. In other words, with the help of polarized entangled state $(|H\rangle_A|V\rangle_B + |V\rangle_A|H\rangle_B)/\sqrt{2}$, the OAM Bell states still cannot be distinguished completely.

To distinguish the OAM Bell states completely, finding a group of suitable projective basis set in the measurement is a key step. First, we can assume them to be $|\psi_1^m\rangle$, $|\psi_2^m\rangle$, $|\psi_3^m\rangle$, and $|\psi_4^m\rangle$, which are linked together with $|\phi_1^m\rangle$, $|\phi_2^m\rangle$, $|\phi_3^m\rangle$, and $|\phi_4^m\rangle$ by a unitary transformation matrix $U(4)$

$$\begin{pmatrix}|\psi_1^m\rangle\\ |\psi_2^m\rangle\\ |\psi_3^m\rangle\\ |\psi_4^m\rangle\end{pmatrix} = U(4)\begin{pmatrix}|\phi_1^m\rangle\\ |\phi_2^m\rangle\\ |\phi_3^m\rangle\\ |\phi_4^m\rangle\end{pmatrix}, \tag{A4a}$$

or

$$\begin{pmatrix}|\phi_1^m\rangle\\ |\phi_2^m\rangle\\ |\phi_3^m\rangle\\ |\phi_4^m\rangle\end{pmatrix} = U(4)^\dagger\begin{pmatrix}|\psi_1^m\rangle\\ |\psi_2^m\rangle\\ |\psi_3^m\rangle\\ |\psi_4^m\rangle\end{pmatrix}. \tag{A4b}$$

Since the determination of $|\psi_k^m\rangle$ $(k = 1, \ldots, 4)$ is followed by $U(4)$, we should research a suitable transformation matrix

$$\frac{1}{\sqrt{2}}\begin{pmatrix}1&1&0&0\\1&-1&0&0\\0&0&1&1\\0&0&1&-1\end{pmatrix}\quad \frac{1}{\sqrt{2}}\begin{pmatrix}0&0&1&-1\\1&-1&0&0\\0&0&1&1\\1&1&0&0\end{pmatrix}\quad \frac{1}{\sqrt{2}}\begin{pmatrix}-1&1&0&0\\0&0&1&-1\\0&0&-1&-1\\-1&-1&0&0\end{pmatrix}\quad \frac{1}{\sqrt{2}}\begin{pmatrix}0&0&-1&1\\-1&1&0&0\\-1&-1&0&0\\0&0&-1&-1\end{pmatrix}$$

$$\frac{1}{\sqrt{2}}\begin{pmatrix}0&0&1&1\\0&0&1&-1\\1&1&0&0\\1&-1&0&0\end{pmatrix}\quad \frac{1}{\sqrt{2}}\begin{pmatrix}0&0&1&1\\1&1&0&0\\0&0&1&-1\\1&-1&0&0\end{pmatrix}\quad \frac{1}{\sqrt{2}}\begin{pmatrix}0&0&-1&-1\\-1&-1&0&0\\-1&1&0&0\\0&0&-1&1\end{pmatrix}\quad \frac{1}{\sqrt{2}}\begin{pmatrix}-1&-1&0&0\\0&0&1&1\\0&0&1&-1\\1&1&0&0\end{pmatrix}$$

FIG. 6. Eight kinds of $U(4)$ satisfying the criterion.

$U_A(4)$ and $U_B(4)$ which can make any one of hyperentangled states ($|\Theta_1^m\rangle$, $|\Theta_2^m\rangle$, $|\Theta_3^m\rangle$, and $|\Theta_4^m\rangle$) be a unique superposition of basis set $\{|\psi_k^m\rangle\}$ $(k = 1, \ldots, 4)$. In other words, with $\{|\psi_k^m\rangle\}$, the simulation results of coincidence measurements should be complete different from every OAM Bell states (this is the criterion).

Since there are a lot of possible $U(4)$, it is not easy to find a suitable one. Reasonably, we can limit $U(4)$ like this: every element of $U(4)$ can only take -1 or 0 or $+1$ and $U_A(4) = U_B(4)$. Now the number of possible matrices is 3^{16}. Our calculation with a MATLAB program shows that there are 384 kinds of $U(4)$ that can satisfy the criterion. Eight of them are shown in Fig. 6.

When the first one is used,

$$U(4) = \frac{1}{\sqrt{2}}\begin{pmatrix}1&1&0&0\\1&-1&0&0\\0&0&1&1\\0&0&1&-1\end{pmatrix}. \tag{A5}$$

The corresponding projective basis set is

$$\begin{pmatrix}|\psi_1^m\rangle\\|\psi_2^m\rangle\\|\psi_3^m\rangle\\|\psi_4^m\rangle\end{pmatrix} = U(4)\begin{pmatrix}|\phi_1^m\rangle\\|\phi_2^m\rangle\\|\phi_3^m\rangle\\|\phi_4^m\rangle\end{pmatrix} = \frac{1}{\sqrt{2}}\begin{pmatrix}|\phi_1^m\rangle + |\phi_2^m\rangle\\|\phi_1^m\rangle - |\phi_2^m\rangle\\|\phi_3^m\rangle + |\phi_4^m\rangle\\|\phi_3^m\rangle - |\phi_4^m\rangle\end{pmatrix}, \tag{A6}$$

which is used in the main text.

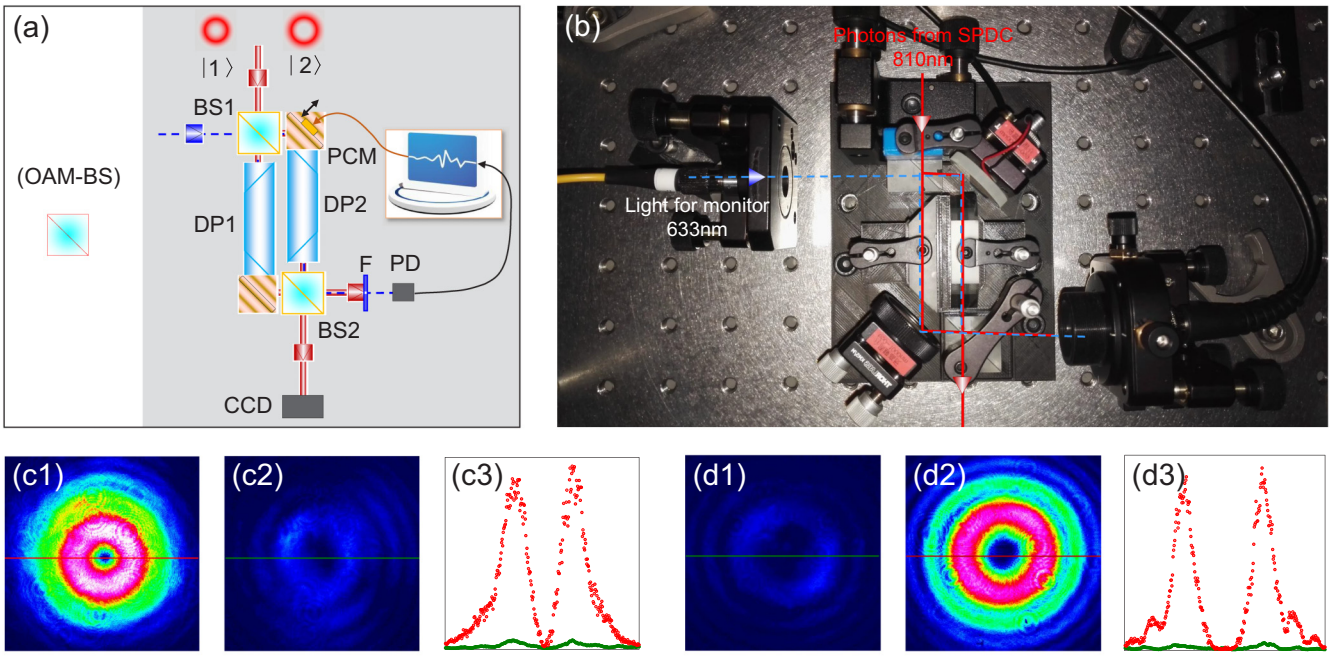

FIG. 7. Test of OAM-BS. (a) Detail on OAM-BS and its function. (b) Photo of arrangement of OAM-BS and its servo system in our experiment. (c1), (c2) Measured patterns of transmitted and reflected light for the input state of $|1\rangle$, respectively. (d1), (d2) Measured patterns of transmitted and reflected light for the input state of $|2\rangle$, respectively. The red curves in panels (c3) and (d3) are taken from the experimental data along the horizontal red lines in panels (c1) and (d2), while the orange curves in panels (c3) and (d3) are taken from the experimental data along the horizontal orange lines in panels (c2) and (d1), respectively.

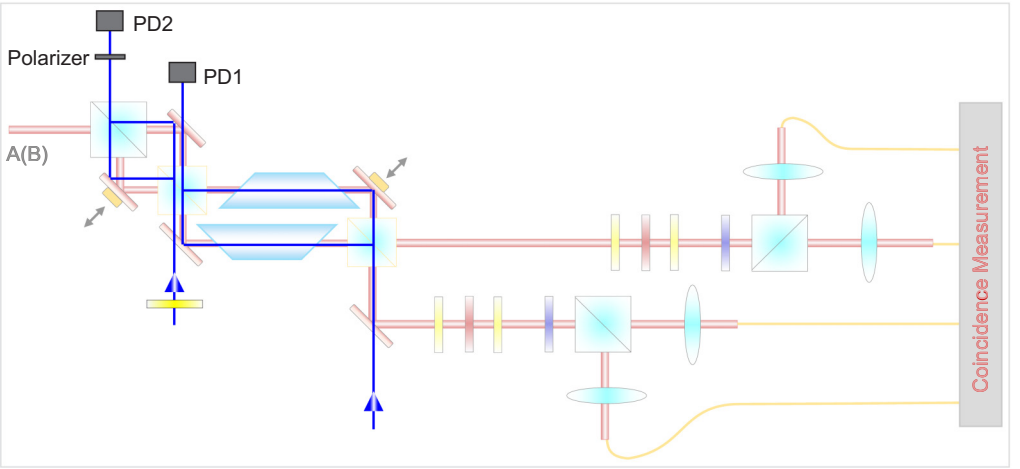

FIG. 8. Servo system in our setup. PD1 is used to stabilize the interferometer composed of two BSs, while PD2 is used to stabilize the interferometer composed of PBS and the first BS.

2. Orbital angular momentum beam splitter and servo system

OAM beam splitter (OAM-BS) is in fact a modified MZ interferometer composed of two mirrors, two BSs, and two Dove prisms (DPs, oriented at an angle of θ with respect to each other). Figures 7(a) and 7(b) show a diagrammatic sketch and an actual photo of the OAM-BS, respectively. The phase different Δ between the two arms of the modified MZ interferometer is adjusted by the piezo controlled mirror (PCM). For the input state $|1\rangle$ (or $|2\rangle$), the transmitted and reflected light will be constructive (destructive) and destructive (constructive) interference, respectively, when setting $\theta = 90^\circ$ and $\Delta = 0$. The interference patterns are shown in Figs. 7(c1), 7(d1), 7(c2), and 7(d2). The red and black curves in Figs. 7(c3) and 7(d3) are the experimental data corresponding to the red lines in Figs. 7(c1) and 7(d2), respectively. The transmittance of $|1\rangle$ and reflectance of $|2\rangle$ are greater than 96%. Setting $\Delta = \pi$ by adjusting the PCM, the transmittance of $|2\rangle$ and reflectance of $|1\rangle$ are also greater than 96%.

In our experiment, there are many modified MZ interferometers (as shown in Fig. 8). In each MZ interferometer, there is an independent servo system, which is a closed loop and composed of light source with a wavelength of 633 nm, a piezo chip, a PCM, a photodiode (PD), and a control program shown in Figs. 7(a) and 7(b). Due to the tiny instability of optical elements, platform, and the disturbance of the environment, the relative optical path difference of the two arms of the MZ interferometer will change slightly, resulting in a slight change in the intensity detected by PD. Then the feedback electric signal provided by the control program will change correspondingly. Finally, the control program will send a corresponding voltage to PCM to compensate for this relative optical path difference.

3. q plate

The q plate plays the key role in our OAM Bell-state analyzer. Generally, the function for a m'-order q plate can

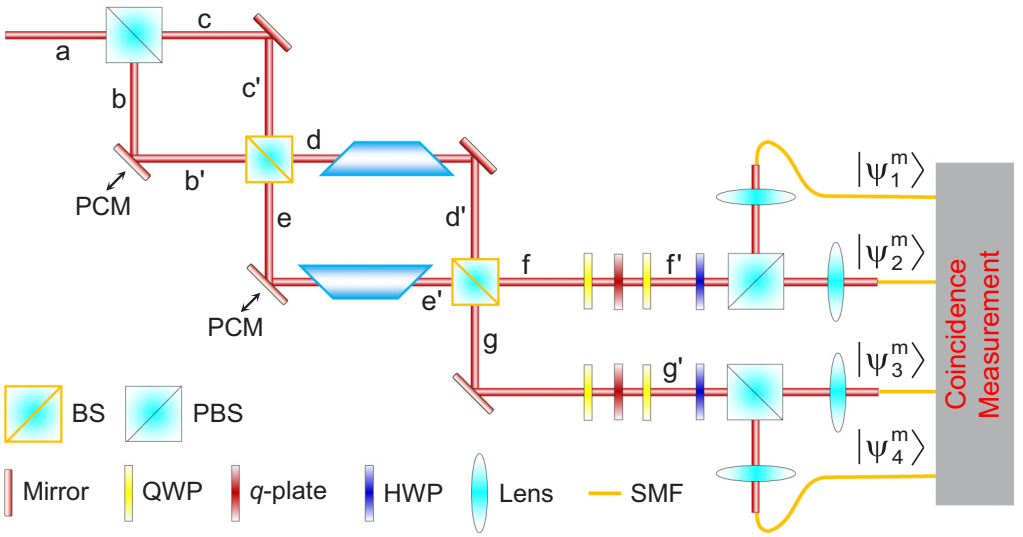

FIG. 9. OAM Bell-state analyzer shown in Fig. 1(c) of the main text.

be described as follows:

$$|R\rangle|m\rangle \xrightarrow{m'/2\text{-order } q \text{ plate}} |L\rangle|m+m'\rangle,$$
$$|L\rangle|m\rangle \xrightarrow{m'/2\text{-order } q \text{ plate}} |R\rangle|m-m'\rangle. \tag{A7}$$

Here, $|R\rangle \propto |H\rangle + j|V\rangle$ and $|L\rangle \propto |H\rangle - j|V\rangle$ represent the right- and left-circularly polarized states, respectively. In this work, some 1/2-order (which can convert the OAM state $|+1\rangle$ or $|-1\rangle$ into the fundamental Gaussian mode state $|0\rangle$) and single-order q plates (which can convert the OAM state $|+2\rangle$ or $|-2\rangle$ into the fundamental Gaussian mode state $|0\rangle$) are used.

4. Evolution of photon states in the orbital angular momentum Bell-state analyzer

The OAM Bell-state analyzer is shown in Fig. 9. Before meeting a polarization beam splitter (PBS), a single photon contains the basis states of $|\phi_k^m\rangle$ $(k = 1, \ldots, 4)$. The function of the PBS is $|x\rangle_a|H\rangle_a \xrightarrow{\text{PBS}} |x\rangle_c|H\rangle_c$ and $|x\rangle_a|V\rangle_a \xrightarrow{\text{PBS}} |-x\rangle_b|V\rangle_b$. The evolution of photon states from b (c) to b' (c') is $|x\rangle_b|y\rangle_b \to e^{jx_1}|-x\rangle_{b'}|y\rangle_{b'}$ $(|x\rangle_c|y\rangle_c \to |-x\rangle_{c'}|y\rangle_{c'})$. Here, $|x\rangle$ represents the OAM state of the photon with OAM $x\hbar$, $y = H$ or $y = V$, and the phase e^{jx_1} is controlled by the piezo-controlled mirror. Similarly, there are $|x\rangle_e|y\rangle_e \to e^{jx_2}|x\rangle_{e'}|y\rangle_{e'}$ and $|x\rangle_d|y\rangle_d \to e^{\text{sgn}(x)j\pi/2}|x\rangle_{d'}|y\rangle_{d'}$, where e^{jx_2} and $e^{\text{sgn}(x)j\pi/2}$ are produced by another the PCM and a pair of Dove prisms (DP4@45°/m and DP5@0°), and sgn$(\cdot)$ is the sign function.

The relationship between two input states (b' and c') and output states (e and f) of BS are $|x\rangle_{b'}|y\rangle_{b'} \xrightarrow{\text{BS}} (|-x\rangle_e|y\rangle_e + |x\rangle_d|y\rangle_d)/\sqrt{2}$ and $|x\rangle_{c'}|y\rangle_{c'} \xrightarrow{\text{BS}} (|x\rangle_e|y\rangle_e - |-x\rangle_d|y\rangle_d)/\sqrt{2}$. Similarly, $|x\rangle_{e'}|y\rangle_{e'} \xrightarrow{\text{BS}} (|-x\rangle_g|y\rangle_g + |x\rangle_f|y\rangle_f)/\sqrt{2}$ and $|x\rangle_{d'}|y\rangle_{d'} \xrightarrow{\text{BS}} (|x\rangle_g|y\rangle_g - |-x\rangle_f|y\rangle_f)/\sqrt{2}$. Finally, the evolution of photon basis set from a to f (g) can be calculated as

$$\begin{aligned}
|-m\rangle_a|H\rangle_a &\xrightarrow{\text{PBS}} |-m\rangle_c|H\rangle_c \longrightarrow |+m\rangle_{c'}|H\rangle_{c'} \xrightarrow{\text{BS}} \frac{1}{\sqrt{2}}(|+m\rangle_e|H\rangle_e - |-m\rangle_d|H\rangle_d)\\
&\longrightarrow \frac{1}{\sqrt{2}}(e^{jx_2}|+m\rangle_{e'}|H\rangle_{e'} - e^{-j\pi/2}|-m\rangle_{d'}|H\rangle_{d'})\\
&\xrightarrow{\text{BS}} \frac{1}{2}[e^{jx_2}(|-m\rangle_g|H\rangle_g + |+m\rangle_f|H\rangle_f) - e^{-j\pi/2}(|-m\rangle_g|H\rangle_g - |+m\rangle_f|H\rangle_f)]\\
&\longrightarrow \frac{1}{2}[(e^{jx_2} - e^{-j\pi/2})|-m\rangle_g|H\rangle_g + (e^{jx_2} + e^{-j\pi/2})|+m\rangle_f|H\rangle_f], \qquad \text{(A8a)}\\
|+m\rangle_a|V\rangle_a &\xrightarrow{\text{PBS}} |-m\rangle_b|V\rangle_b \longrightarrow e^{jx_1}|+m\rangle_{b'}|V\rangle_{b'} \xrightarrow{\text{BS}} \frac{1}{\sqrt{2}}e^{jx_1}(|-m\rangle_e|V\rangle_e + |+m\rangle_d|V\rangle_d)\\
&\longrightarrow \frac{1}{\sqrt{2}}e^{jx_1}(e^{jx_2}|-m\rangle_{e'}|V\rangle_{e'} - e^{+j\pi/2}|+m\rangle_{d'}|V\rangle_{d'})\\
&\xrightarrow{\text{BS}} \frac{1}{2}e^{jx_1}[e^{jx_2}(|+m\rangle_g|V\rangle_g + |-m\rangle_f|V\rangle_f) + e^{+j\pi/2}(|+m\rangle_g|V\rangle_g - |-m\rangle_f|V\rangle_f)]\\
&\longrightarrow \frac{1}{2}e^{jx_1}[(e^{jx_2} + e^{+j\pi/2})|+m\rangle_g|V\rangle_g + (e^{jx_2} - e^{+j\pi/2})|-m\rangle_f|V\rangle_f], \qquad \text{(A8b)}\\
|-m\rangle_a|V\rangle_a &\xrightarrow{\text{PBS}} |+m\rangle_b|V\rangle_b \longrightarrow e^{jx_1}|-m\rangle_{b'}|V\rangle_{b'} \xrightarrow{\text{BS}} \frac{1}{\sqrt{2}}e^{jx_1}(|+m\rangle_e|V\rangle_e + |-m\rangle_d|V\rangle_d)\\
&\longrightarrow \frac{1}{\sqrt{2}}e^{jx_1}(e^{jx_2}|+m\rangle_{e'}|V\rangle_{e'} + e^{-j\pi/2}|-m\rangle_{d'}|V\rangle_{d'})\\
&\xrightarrow{\text{BS}} \frac{1}{2}e^{jx_1}[e^{jx_2}(|-m\rangle_g|V\rangle_g + |+m\rangle_f|V\rangle_f) + e^{-j\pi/2}(|-m\rangle_g|V\rangle_g - |+m\rangle_f|V\rangle_f)]\\
&\longrightarrow \frac{1}{2}e^{jx_1}[(e^{jx_2} + e^{-j\pi/2})|-m\rangle_g|V\rangle_g + (e^{jx_2} - e^{-j\pi/2})|+m\rangle_f|V\rangle_f], \qquad \text{(A8c)}\\
|+m\rangle_a|H\rangle_a &\xrightarrow{\text{PBS}} |+m\rangle_c|H\rangle_c \longrightarrow |-m\rangle_{c'}|H\rangle_{c'} \xrightarrow{\text{BS}} \frac{1}{\sqrt{2}}(|-m\rangle_e|H\rangle_e - |+m\rangle_d|H\rangle_d)\\
&\longrightarrow \frac{1}{\sqrt{2}}(e^{jx_2}|-m\rangle_{e'}|H\rangle_{e'} - e^{+j\pi/2}|+m\rangle_{d'}|H\rangle_{d'})\\
&\xrightarrow{\text{BS}} \frac{1}{2}[e^{jx_2}(|+m\rangle_g|H\rangle_g + |-m\rangle_f|H\rangle_f) - e^{+j\pi/2}(|+m\rangle_g|H\rangle_g - |-m\rangle_f|H\rangle_f)]\\
&\longrightarrow \frac{1}{2}[(e^{jx_2} - e^{+j\pi/2})|+m\rangle_g|H\rangle_g + (e^{jx_2} + e^{+j\pi/2})|-m\rangle_f|H\rangle_f]. \qquad \text{(A8d)}
\end{aligned}$$

Setting $e^{jx_1}=1$ and $e^{jx_2}=e^{-j\pi/2}$, we can obtain that $|-m\rangle_a|H\rangle_a \to |+m\rangle_f|H\rangle_f$, $|+m\rangle_a|V\rangle_a \to |-m\rangle_f|V\rangle_f$, $|-m\rangle_a|V\rangle_a \to |-m\rangle_g|V\rangle_g$, and $|+m\rangle_a|H\rangle_a \to |+m\rangle_g|H\rangle_g$. Then a $m/2$-order q plate sandwiched by two quarter-wave plates (QWPs) can transform the states f (g) into f' (g') as

$$|+m\rangle_{g(f)}|H\rangle_{g(f)} \xrightarrow{\text{QWP1}} |+m\rangle|R\rangle \xrightarrow{q-\text{plate}} |0\rangle|L\rangle \xrightarrow{\text{QWP2}} |0\rangle_{g'(f')}|V\rangle_{g'(f')}, \tag{A9a}$$

$$|-m\rangle_{g(f)}|V\rangle_{g(f)} \xrightarrow{\text{QWP1}} |-m\rangle|L\rangle \xrightarrow{q-\text{plate}} |0\rangle|R\rangle \xrightarrow{\text{QWP2}} |0\rangle_{g'(f')}|H\rangle_{g'(f')}. \tag{A9b}$$

So we have

$$|-m\rangle_a|H\rangle_a + |+m\rangle_a|V\rangle_a \longleftrightarrow |V\rangle_{f'} + |H\rangle_{f'} \longleftrightarrow +|\nearrow\rangle_{f'} \longleftrightarrow |\psi_1^m\rangle, \tag{A10a}$$

$$|-m\rangle_a|H\rangle_a - |+m\rangle_a|V\rangle_a \longleftrightarrow |V\rangle_{f'} - |H\rangle_{f'} \longleftrightarrow -|\searrow\rangle_{f'} \longleftrightarrow |\psi_2^m\rangle, \tag{A10b}$$

$$|-m\rangle_a|V\rangle_a + |+m\rangle_a|H\rangle_a \longleftrightarrow |V\rangle_{g'} + |H\rangle_{g'} \longleftrightarrow +|\nearrow\rangle_{g'} \longleftrightarrow |\psi_3^m\rangle, \tag{A10c}$$

$$|-m\rangle_a|V\rangle_a - |+m\rangle_a|V\rangle_a \longleftrightarrow |V\rangle_{g'} - |H\rangle_{g'} \longleftrightarrow -|\searrow\rangle_{g'} \longleftrightarrow |\psi_4^m\rangle. \tag{A10d}$$

Here, $|\nearrow\rangle \propto (|H\rangle + |V\rangle)$ and $|\searrow\rangle \propto (|H\rangle - |V\rangle)$ which can be separated with a HWP@22.5° and a PBS. These results demonstrate that our experimental setup plays the role of the unitary transformation matrix $U(4)$ shown in Eqs. (A5) and (A6). So, after passing through the whole setup, we have

$$\begin{aligned}
|\Theta_1^m\rangle =& \tfrac{1}{2}(|-m\rangle_{Aa}|H\rangle_{Aa}|+m\rangle_{Ba}|V\rangle_{Ba} + |-m\rangle_{Aa}|V\rangle_{Aa}|+m\rangle_{Ba}|H\rangle_{Ba} \\
&+ |+m\rangle_{Aa}|H\rangle_{Aa}|-m\rangle_{Ba}|V\rangle_{Ba} + |+m\rangle_{Aa}|V\rangle_{Aa}|-m\rangle_{Ba}|H\rangle_{Ba}) \\
\xrightarrow{\text{PBS+OAM-BS}}& \tfrac{1}{2}(|-m\rangle_{Af}|H\rangle_{Af}|+m\rangle_{Bf}|V\rangle_{Bf} + |+m\rangle_{Ag}|V\rangle_{Ag}|-m\rangle_{Bg}|H\rangle_{Bg} \\
&+ |-m\rangle_{Ag}|H\rangle_{Ag}|+m\rangle_{Bg}|V\rangle_{Bg} + |+m\rangle_{Af}|V\rangle_{Af}|-m\rangle_{Bf}|H\rangle_{Bf}) \\
\xrightarrow{\text{QWP+}q\text{ plate+QWP}}& -\tfrac{1}{2}|0\rangle_A|0\rangle_B(|V\rangle_{Af'}|H\rangle_{Bf'} + |H\rangle_{Ag'}|V\rangle_{Bg'} + |V\rangle_{Ag'}|H\rangle_{Bg'} + |H\rangle_{Af'}|V\rangle_{Bf'}) \\
\xrightarrow{\text{HWP@22.5}^\circ\text{+PBS}}& +\tfrac{1}{2}\left(|\psi_1^m\rangle_A|\psi_1^m\rangle_B - |\psi_2^m\rangle_A|\psi_2^m\rangle_B + |\psi_3^m\rangle_A|\psi_3^m\rangle_B - |\psi_4^m\rangle_A|\psi_4^m\rangle_B\right).
\end{aligned} \tag{A11a}$$

Similarly, we have

$$|\Theta_2^m\rangle \to +\tfrac{1}{2}\left(|\psi_2^m\rangle_A|\psi_1^m\rangle_B - |\psi_1^m\rangle_A|\psi_2^m\rangle_B + |\psi_4^m\rangle_A|\psi_3^m\rangle_B - |\psi_3^m\rangle_A|\psi_4^m\rangle_B\right), \tag{A11b}$$

$$|\Theta_3^m\rangle \to +\tfrac{1}{2}\left(|\psi_3^m\rangle_A|\psi_1^m\rangle_B + |\psi_4^m\rangle_A|\psi_2^m\rangle_B + |\psi_1^m\rangle_A|\psi_3^m\rangle_B + |\psi_2^m\rangle_A|\psi_4^m\rangle_B\right), \tag{A11c}$$

$$|\Theta_4^m\rangle \to -\tfrac{1}{2}\left(|\psi_4^m\rangle_A|\psi_1^m\rangle_B + |\psi_3^m\rangle_A|\psi_2^m\rangle_B + |\psi_2^m\rangle_A|\psi_3^m\rangle_B + |\psi_1^m\rangle_A|\psi_4^m\rangle_B\right). \tag{A11d}$$

[1] M. J. Collins, C. Xiong, I. H. Rey, T. D. Vo, J. He, S. Shahnia, C. Reardon, T. F. Krauss, M. J. Steel, A. S. Clark, and B. J. Eggleton, Integrated spatial multiplexing of heralded single-photon sources, Nat. Commun. **4**, 2582 (2013).

[2] L. Mazzarella, F. Ticozzi, A. V. Sergienko, G. Vallone, and P. Villoresi, Asymmetric architecture for heralded single-photon sources, Phys. Rev. A **88**, 023848 (2013).

[3] F. Kaneda, B. G. Christensen, J. J. Wong, H. S. Park, K. T. McCusker, and P. G. Kwiat, Time-multiplexed heralded single-photon source, Optica **2**, 1010 (2015).

[4] C. Xiong, X. Zhang, Z. Liu, M. J. Collins, A. Mahendra, L. Helt, M. Steel, D.-Y. Choi, C. Chae, P. H. W. Leong, and B. J. Eggleton, Active temporal multiplexing of indistinguishable heralded single photons, Nat. Commun. **7**, 10853 (2016).

[5] C. Joshi, A. Farsi, S. Clemmen, S. Ramelow, and A. L. Gaeta, Frequency multiplexing for quasi-deterministic heralded single-photon sources, Nat. Commun. **9**, 847 (2018).

[6] L. Allen, M. W. Beijersbergen, R. J. C. Spreeuw, and J. P. Woerdman, Orbital angular momentum of light and the transformation of Laguerre-Gaussian laser modes, Phys. Rev. A **45**, 8185 (1992).

[7] A. Mair, A. Vaziri, G. Weihs, and A. Zeilinger, Entanglement of the orbital angular momentum states of photons, Nature (London) **412**, 313 (2001).

[8] J. Leach, B. Jack, J. Romero, A. K. Jha, A. M. Yao, S. Franke-Arnold, D. G. Ireland, R. W. Boyd, S. M. Barnett, and M. J. Padgett, Quantum correlations in optical angle-orbital angular momentum variables, Science **329**, 662 (2010).

[9] G. Molina-Terriza, A. Vaziri, J. Řeháček, Z. Hradil, and A. Zeilinger, Triggered Qutrits for Quantum Communication Protocols, Phys. Rev. Lett. **92**, 167903 (2004).

[10] N. K. Langford, R. B. Dalton, M. D. Harvey, J. L. O'Brien, G. J. Pryde, A. Gilchrist, S. D. Bartlett, and A. G. White, Measuring Entangled Qutrits and Their Use for Quantum Bit Commitment, Phys. Rev. Lett. **93**, 053601 (2004).

[11] V. D. Salakhutdinov, E. R. Eliel, and W. Löffler, Full-Field Quantum Correlations of Spatially Entangled Photons, Phys. Rev. Lett. **108**, 173604 (2012).

[12] E. Nagali, L. Sansoni, F. Sciarrino, F. D. Martini, L. Marrucci, B. Piccirillo, E. Karimi, and E. Santamato, Optimal quantum cloning of orbital angular momentum photon qubits through Hong-Ou-Mandel coalescence, Nat. Photonics **3**, 720 (2009).

[13] R. Fickler, R. Lapkiewicz, W. N. Plick, M. Krenn, C. Schaeff, S. Ramelow, and A. Zeilinger, Quantum entanglement of high angular momenta, Science **338**, 640 (2012).

[14] T. M. Graham, H. J. Bernstein, T. C. Wei, M. Junge, and P. G. Kwiat, Superdense teleportation using hyperentangled photons, Nat. Commun. **6**, 7185 (2015).

[15] N. Uribe-Patarroyo, A. Fraine, D. S. Simon, O. Minaeva, and A. V. Sergienko, Object Identification Using Correlated Orbital Angular Momentum States, Phys. Rev. Lett. **110**, 043601 (2013).

[16] Z. Q. Zhou, Y. L. Hua, X. Liu, G. Chen, J. S. Xu, Y. J. Han, C. F. Li, and G. C. Guo, Quantum Storage of Three-Dimensional Orbital-Angular-Momentum Entanglement in a Crystal, Phys. Rev. Lett. **115**, 070502 (2015).

[17] B. C. Hiesmayr, M. J. A. de Dood, and W. Löffler, Observation of Four-Photon Orbital Angular Momentum Entanglement, Phys. Rev. Lett. **116**, 073601 (2016).

[18] A. C. Dada, J. Leach, G. S. Buller, M. J. Padgett, and E. Andersson, Experimental high-dimensional two-photon entanglement and violations of generalized Bell inequalities, Nat. Phys. **7**, 677 (2011).

[19] M. Malik, M. Erhard, M. Huber, M. Krenn, R. Fickler, and A. Zeilinger, Multi-photon entanglement in high dimensions, Nat. Photonics **10**, 248 (2016).

[20] Y. Zhang, F. S. Roux, T. Konrad, M. Agnew, J. Leach, and A. Forbes, Engineering two-photon high-dimensional states through quantum interference, Sci. Adv. **2**, e1501165 (2016).

[21] J. T. Barreiro, T. C. Wei, and P. G. Kwiat, Beating the channel capacity limit for linear photonic superdense coding, Nat. Phys. **4**, 282 (2008).

[22] J. T. Barreiro, N. K. Langford, N. A. Peters, and P. G. Kwiat, Generation of Hyperentangled Photon Pairs, Phys. Rev. Lett. **95**, 260501 (2005).

[23] J. Leach, M. J. Padgett, S. M. Barnett, S. Franke-Arnold, and J. Courtial, Measuring the Orbital Angular Momentum of a Single Photon, Phys. Rev. Lett. **88**, 257901 (2002).

[24] L. Marrucci, C. Manzo, and D. Paparo, Optical Spin-to-Orbital Angular Momentum Conversion in Inhomogeneous Anisotropic Media, Phys. Rev. Lett. **96**, 163905 (2006).

[25] P. Chen, W. Ji, B. Y. Wei, W. Hu, V. Chigrinov, and Y. Q. Lu, Generation of arbitrary vector beams with liquid crystal polarization converters and vector-photoaligned *q*-plates, Appl. Phys. Lett. **107**, 241102 (2015).

[26] L. Dominici, G. Dagvadorj, J. M. Fellows, D. Ballarini, M. D. Giorgi, F. M. Marchetti, B. Piccirillo, L. Marrucci, A. Bramati, G. Gigli, M. H. Szymańska, and D. Sanvitto, Vortex and half-vortex dynamics in a nonlinear spinor quantum fluid, Sci. Adv. **1**, e1500807 (2015).

[27] M. Krenn, R. Fickler, M. Fink, J. Handsteiner, M. Malik, T. Scheidl, R. Ursin, and A. Zeilinger, Communication with spatially modulated light through turbulent air across Vienna, New J. Phys. **16**, 113028 (2014).

[28] Y. Ren, G. Xie, H. Huang, C. Bao, Y. Yan, N. Ahmed, M. P. J. Lavery, B. I. Erkmen, S. Dolinar, M. Tur, M. A. Neifeld, M. J. Padgett, R. W. Boyd, J. H. Shapiro, and A. E. Willner, Adaptive optics compensation of multiple orbital angular momentum beams propagating through emulated atmospheric turbulence, Opt. Lett. **39**, 2845 (2014).

[29] B. Ndagano, B. Perez-Garcia, F. S. Roux, M. McLaren, C. Rosales-Guzman, Y. Zhang, O. Mouane, R. I. Hernandez-Aranda, T. Konrad, and A. Forbes, Characterizing quantum channels with non-separable states of classical light, Nat. Phys. **13**, 397 (2017).

[30] N. Bozinovic, Y. Yue, Y. Ren, M. Tur, P. Kristensen, H. Huang, A. E. Willner, and S. Ramachandran, Terabit-scale orbital angular momentum mode division multiplexing in fibers, Science, **340**, 1545 (2013).

[31] S. Li, Q. Mo, X. Hu, C. Du, and J. Wang, Controllable all-fiber orbital angular momentum mode converter, Opt. Lett. **40**, 4376 (2015).

[32] K. Mattle, H. Weinfurter, P. G. Kwiat, and A. Zeilinger, Dense Coding in Experimental Quantum Communication, Phys. Rev. Lett. **76**, 4656 (1996).

[33] B. P. Williams, R. J. Sadlier, and T. S. Humble, Superdense Coding Over Optical Fiber Links with Complete Bell-State Measurements, Phys. Rev. Lett. **118**, 050501 (2017).

[34] D. Bouwmeester, J. W. Pan, K. Mattle, M. Eibl, H. Weinfurter, and A. Zeilinger, Experimental quantum teleportation, Nature (London) **390**, 575 (1997).

[35] D. Boschi, S. Branca, F. De Martini, L. Hardy, and S. Popescu, Experimental Realization of Teleporting an Unknown Pure Quantum State Via Dual Classical and Einstein-Podolsky-Rosen Channels, Phys. Rev. Lett. **80**, 1121 (1998).

[36] X. L. Wang, X. D. Cai, Z. E. Su, M. C. Chen, D. Wu, L. Li, N. L. Liu, C. Y. Lu, and J. W. Pan, Quantum teleportation of multiple degrees of freedom of a single photon, Nature (London) **518**, 516 (2015).

[37] M. Zukowski, A. Zeilinger, M. A. Horne, and A. K. Ekert, "Event-Ready-Detectors" Bell Experiment Via Entanglement Swapping, Phys. Rev. Lett. **71**, 4287 (1993).

[38] J. W. Pan, D. Bouwmeester, H. Weinfurter, and A. Zeilinger, Experimental Entanglement Swapping: Entangling Photons that Never Interacted, Phys. Rev. Lett. **80**, 3891 (1998).

[39] Y. Zhang, M. Agnew, T. Roger, F. S. Roux, T. Konrad, D. Faccio, J. Leach, and A. Forbes, Simultaneous entanglement swapping of multiple orbital angular momentum states of light, Nat. Commun. **8**, 632 (2017).